

Abnormal Pressure-Induced Photoluminescence Enhancement and Phase Decomposition in Pyrochlore

$\text{La}_2\text{Sn}_2\text{O}_7$

HPSTAR
396-2017

Yongsheng Zhao, Nana Li, Cong Xu, Yan Li, Hongyu Zhu, Pinwen Zhu, Xin Wang,*
and Wenge Yang*

Dedicated to Prof. Guangtian Zou on the occasion of his 80th birthday

$\text{La}_2\text{Sn}_2\text{O}_7$ is a transparent conducting oxide (TCO) material and shows a strong near-infrared fluorescent at ambient pressure and room temperature. By in situ high-pressure research, pressure-induced visible photoluminescence (PL) above 2 GPa near 2 eV is observed. The emergence of unusual visible PL behavior is associated with the seriously trigonal lattice distortion of the SnO_6 octahedra, under which the Sn–O–Sn exchange angle θ is decreased below 22.1 GPa, thus enhancing the PL quantum yield leading to $\text{Sn } ^3\text{P}_1 \rightarrow ^1\text{S}_0$ photons transition. Besides, bandgap closing followed by bandgap opening and the visible PL appearing at the point of the gap reversal, which is consistent with high-pressure phase decomposition, are discovered. The high-pressure PL results demonstrate a well-defined pressure window (7–17 GPa) with flat maximum PL yielding and sharp edges at both ends, which may provide a great calibration tool for pressure sensors for operation in the deep sea or at extreme conditions.

Optical pressure sensors have gained great interest due to their low electronic noise and demonstrable potential for a wide range of applications. Although poly(dimethylsiloxane) film is an ideal material for fabricating flexible optical pressure sensors that can be deposited on a flexible substrate for both electronic-skin and physiological measurement applications, these devices have limited availability. Therefore, investigating a material

with good structural stability, chemical durability, and radiation tolerance under extreme conditions is necessary for developing new pressure sensors.^[1] Pyrochlore $\text{A}_2\text{B}_2\text{O}_7$ is a potential candidate for permanently disposing of high-level radioactive waste in safe geologic repositories due to its chemical stability, low swelling, and excellent radiation tolerance.^[2,3] Also, pyrochlore is an attractive material because of its complex magnetic properties.^[4] A pressure-induced spin transition, bandgap change, and lattice distortion have been reported in some pyrochlores before, but no study has solely focused on the effect of photoluminescence (PL) in the pyrochlore system.^[5–7] However, we previously reported a PL change with pressure in a pyrochlore, $\text{Eu}_2\text{Sn}_2\text{O}_7$, which exhibited an interesting pressure-dependent evolution

of the Eu^{3+} 4f electronic structure.^[8] Even though the luminescence properties of ns^2 ions have been extensively studied, near-infrared (NIR) region PL is rarely observed in BaSnO_3 .^[9] To improve the PL efficiency, the d transition metal, and p block elements can be utilized as primary activators in doped pyrophosphates.^[10] In fact, the Mn^{2+} ion itself is an efficient PL center and PL can emerge or be quenched by pressure-induced structural transitions.^[11] Therefore, a change in the lattice symmetry and local coordination environment are important for modifying PL by pressure and the reduction of excited charge migration through the Mn–F–Mn exchange pathway provides the possibility of pressure-induced PL. At ambient conditions, two emission peaks related to the oxygen vacancies and defects were observed in nanostructured SnO_2 , while pressure-induced PL emergence and quench were observed in MnF_2 and SnBr_4 due to phase transitions.^[11–13]

$\text{La}_2\text{Sn}_2\text{O}_7$ is a transparent conducting oxide (TCO) material with a $4d^{10}5s^0$ electron configuration in the Sn^{4+} ion and has potential applications as thin film devices like light-emitting diodes and electroluminescent flat panel displays.^[14] In the $\text{La}_2\text{Sn}_2\text{O}_7$ system, La^{3+} does not have a 4f electron, so PL originating from the f electron transition is unexpected at ambient pressure and room temperature (RT). Since the majority of PL emissions in rare earth ions originate from their f electron

Dr. Y. S. Zhao, Dr. Y. Li, Dr. H. Y. Zhu, Prof. P. W. Zhu, Prof. X. Wang
State Key Laboratory of Superhard Materials
Department of Physics
Jilin University
Changchun 130012, China
E-mail: xin_wang@jlu.edu.cn

Dr. Y. S. Zhao, Dr. N. N. Li, C. Xu, Prof. W. G. Yang
Center for High Pressure Science and Technology Advanced Research (HPSTAR)
Shanghai 201203, China
E-mail: yangwg@hpstar.ac.cn, wyang@carnegiescience.edu
Prof. W. G. Yang
High Pressure Synergetic Consortium (HPSynC)
Geophysical Laboratory
Carnegie Institution of Washington
Argonne, IL 60439, USA

DOI: 10.1002/adma.201701513

transition,^[15] the strong room-temperature NIR luminescence at 804 nm may be associated with the Sn^{2+} ions in $\text{La}_2\text{Sn}_2\text{O}_7$. When subjected to high pressure, a novel pressure-induced PL was observed in TCO material $\text{La}_2\text{Sn}_2\text{O}_7$ at RT. An anomalous bandgap closure followed by bandgap opening occurred upon compression, while visible multiband PL near 676 nm appeared at the turning point of the gap reversal above 2 GPa. To elucidate the pressure effect on PL, we conducted a systematic investigation of the high-pressure crystal and electronic structure using in situ angle-dispersive X-ray diffraction (ADXRD), Raman and fluorescence spectrum, impedance, and density functional theory (DFT) calculations. Photoluminescence is invaluable for the development of new, chemically durable, radiation-tolerant hosts for safe and reliable optical pressure sensors to work in deep sea or extreme environments.

The room-temperature PL of $\text{La}_2\text{Sn}_2\text{O}_7$ at 804 nm (1.54 eV) was recorded at ambient pressure as shown in Figure 1a. With increasing pressure, the NIR luminescence signal showed a blue shift to 760 nm (1.63 eV) (inset) and quenched when pressure exceeded 7.3 GPa. The NIR PL originated from the recombination of a photogenerated valence-band hole and an occupied donor level like BaSnO_3 , where the NIR PL was associated with Sn^{2+} ion defect levels located between the bandgap.^[9] This explanation was verified by X-ray photoelectron spectroscopy (XPS) performed on $\text{La}_2\text{Sn}_2\text{O}_7$ (Figure S1, Supporting Information). The Sn^{2+} ion derives from high-temperature annealing, along with the generation of oxygen vacancies, which can be presented by the defect formula: $\text{La}_2(\text{Sn}^{4+}\text{Sn}^{2+})_2\text{O}_{7-x}\square_x$. The pressure-induced visible PL observed at RT above 2 GPa is

shown in Figure 1b. The PL spectrum consisted of two narrow bands between 660 and 700 nm with several other small peaks (we believe the visible PL is associated with a change of the crystal environment of the Sn^{2+} ions) and another peak near 635 nm. The variation of the visible PL spectrum intensity with pressure plateaued between 6.6 and 16.6 GPa, which illustrates a well-defined pressure window that yielded flat maximum PL (Figure 1c). Note that the visible PL showed redshift with pressure and finally disappeared above 23.7 GPa, as shown in the Figure 1c inset. After releasing pressure, the visible PL recovered near 21 GPa and the PL intensity enhanced with decreasing pressure until 7.1 GPa before we lost the PL signal as pressure decreased to 4.8 GPa. The NIR PL did not revert to its original intensity until it had relaxed for at least 1 d. Although the visible PL quenched with higher pressure, our observation of pressure-induced narrow-band visible PL above 2 GPa and the room-temperature NIR PL in $\text{La}_2\text{Sn}_2\text{O}_7$ is noteworthy. To find the source of this PL, we investigated the structural evolution of $\text{La}_2\text{Sn}_2\text{O}_7$ at high pressure using in situ angle-dispersive X-ray diffraction.

$\text{La}_2\text{Sn}_2\text{O}_7$ crystallizes in space group $Fd-3m$ and its crystal structure is shown in Figure S2 (Supporting Information).^[4,16] The tungsten bronze-like Sn_2O_6 component consists of corner-sharing SnO_6 octahedra that form a 3D network of six-membered rings. As shown in Figure S2 (Supporting Information), the Sn_4O tetrahedron connect with each other by Sn^{4+} ions and the $\text{Sn}-\text{O}-\text{Sn}$ rings form a hexagram, while the $\text{La}_2\text{O}'(\text{O}2)$ network has linear $\text{O}2-\text{La}-\text{O}2$ bonds. The pressure-dependent X-ray diffraction patterns shown in Figure 2a did not reveal any

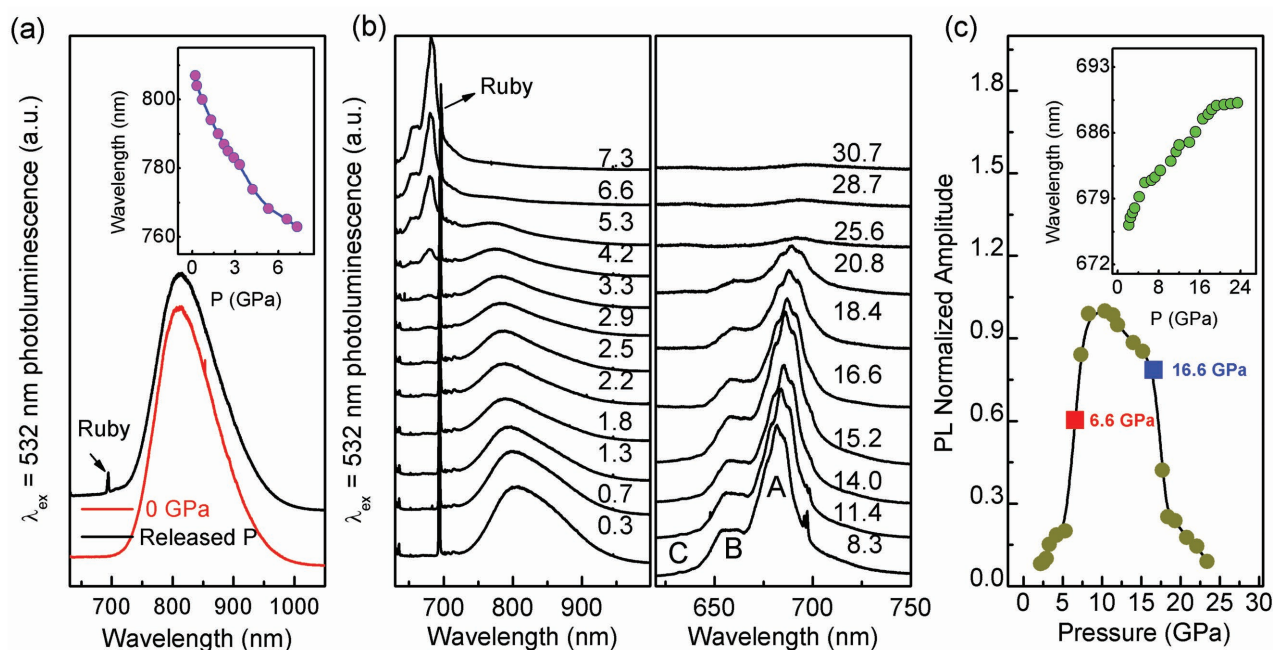


Figure 1. a) Strong room-temperature NIR PL at ambient pressure (red line). After decompression for 1 d, it fully reverted (black line). The inset shows the NIR PL blueshifts with pressure. b) Pressure-induced novel visible PL. The variation of the $\text{La}_2\text{Sn}_2\text{O}_7$ emission spectrum with pressure illustrates PL appearance and quenching. The multiband peaks corresponding to the A band 681 nm ($^1\text{S}_0 \rightarrow ^3\text{P}_1$), B band ($^1\text{S}_0 \rightarrow ^3\text{P}_2$) at 659 nm, and C band ($^1\text{S}_0 \rightarrow ^1\text{P}_1$) at 635 nm in $\text{La}_2\text{Sn}_2\text{O}_7$ are classified as an s^2 - sp transition. c) PL-normalized amplitude depends on pressure; the intensity of the PL reaches an obvious maximum at 9.5 GPa, then drops quickly above 16.6 GPa. In the inset, we draw pressure effect of the strongest peak in A band, note that the visible PL redshifts with increasing pressure and is quenched at 25 GPa.

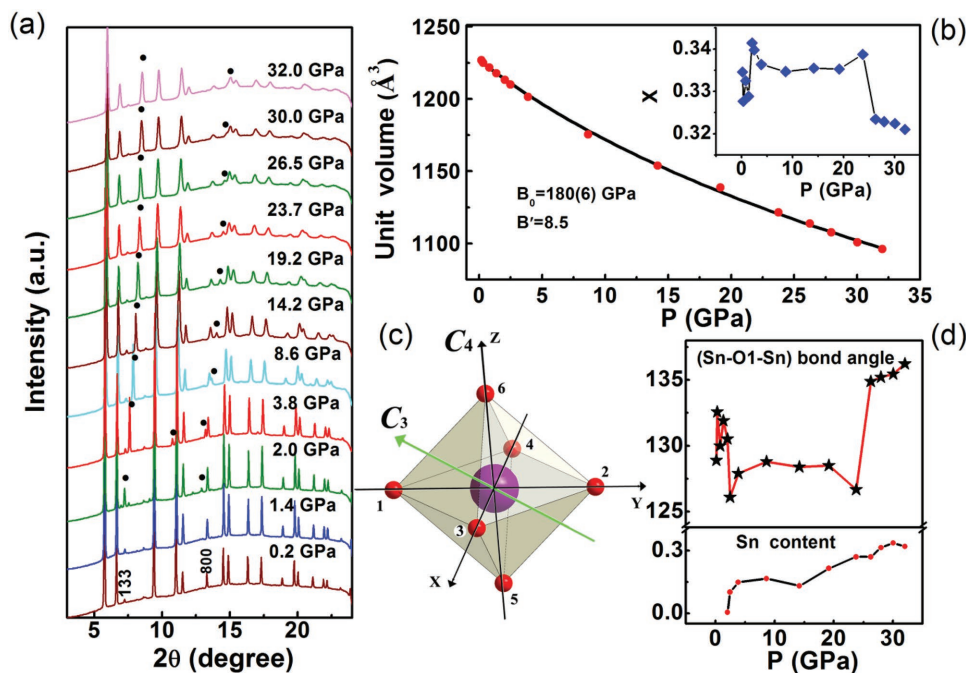


Figure 2. Structural evolution of $\text{La}_2\text{Sn}_2\text{O}_7$ probed by synchrotron XRD at RT and high pressure. a) Angle-dispersive XRD patterns of $\text{La}_2\text{Sn}_2\text{O}_7$ at selected pressures. The black spot peaks are contributed by metallic Sn due to phase decomposition. b) Unit cell volume obtained from Rietveld refinement of powder XRD patterns as a function of pressure. The inset shows the fitting parameter x versus pressure, where the x value is discontinuous at 2 GPa and suddenly drops at 23.7 GPa corresponding to the phase decomposition and phase transition pressure. c) Trigonal crystal field around Sn^{4+} ion and local geometry of a SnO_6 octahedron. A trigonal distortion is induced by compression or elongation of the surrounding oxygen octahedron along the C_3 symmetry axis. d) Top panel: the Sn–O–Sn bond angle θ at varied pressure; note that θ value discontinues at 2 and 23.7 GPa. Bottom panel: metal Sn content in pyrochlore $\text{La}_2\text{Sn}_2\text{O}_7$.

crystallographic symmetry change up to 32 GPa. Nevertheless, there were small amounts of metallic Sn phase decomposition at 2 GPa. Two low-intensity peaks appeared at 2 GPa, marked by dark spots near (133) and (800); the diffraction peaks of $\text{La}_2\text{Sn}_2\text{O}_7$, respectively. These two new peaks could be indexed with the pyrochlore structure and they persisted to the highest pressure of 32 GPa. Comparing these peaks with the diffraction maximum of pyrochlore, the d value changed significantly with pressure and the strongest peak was slightly lower than the maximum diffraction of metallic Sn ($d_{110} = 2.324 \text{ \AA}$). We refined the ADXRD patterns with GSAS Software^[17] based on mixed phases of $\text{La}_2\text{Sn}_2\text{O}_7$ and Sn, yielding a composition of $\approx 10\%$ metallic Sn at 2.5 GPa. The particle size of metallic Sn was 6 nm derived by the Scherrer formula. The refined lattice parameter of the bcc Sn was 3.346 Å at 2 GPa, which is slightly compressed from the reference value of 3.354 Å at ambient conditions.^[18] The V – P plots of $\text{La}_2\text{Sn}_2\text{O}_7$ and Sn were fitted with a third-order Birch–Murnaghan equation of state (EOS), as shown in Figure 2b and Figure S3a (Supporting Information), which yielded a bulk modulus of B_0 180(6) GPa with $B' = 8.5$ for $\text{La}_2\text{Sn}_2\text{O}_7$ up to the highest pressure 32 GPa. In pyrochlore, the only flexible structure parameter x of the oxygen O1 position jumped from 0.329 to 0.341 at 2 GPa (inset in Figure 2b), which indicated pressure-enhanced SnO_6 octahedral distortion. As x deviated from the perfect value of 0.3125, trigonal lattice distortion subsequently enhanced through the compression or elongation of the SnO_6 octahedra along the C_3 symmetry axis (Figure 2c). The change of x was due to

phase decomposition where a small amount of Sn atoms deviated from their symmetry position and consequently formed metallic Sn nanoparticles; thus, the site 16c formation vacancies lead the SnO_6 octahedra to adjust the lattice symmetry. The pressure-enhanced trigonal lattice distortion can induce a full gap opening at the Fermi energy that leads to an insulating phase.^[19] With further compression, the position parameter x slightly decreased then remained stable until 23.7 GPa, as did the Sn content between this pressure range (Figure 2d). The abrupt change of the oxygen atomic position x above 23.7 GPa indicated SnO_6 octahedral rearrangement, which has also been observed in $\text{Gd}_2\text{Ti}_2\text{O}_7$ and $\text{Tb}_2\text{Ti}_2\text{O}_7$.^[20,21] Furthermore, our detailed structural analysis verified the rearrangement of the SnO_6 octahedron, which is reflected in the observed discontinuities of the Sn–O–Sn bond angle (Figure 2d). The distorted SnO_6 octahedron compressed more easily than the unit cell between 2 and 23.7 GPa, as demonstrated by the obvious jump at 2 GPa and sudden drop at 23.7 GPa of the normalized volumes of SnO_6 , but the opposite was true below 2 GPa and above 23.7 GPa (Figure S3, Supporting Information). Therefore, these results suggest a subtle structural deformation above 23.7 GPa. This may be caused by increased vacancies at the 16c site due to the Sn content increase above this pressure. Two Rietveld refinements of $\text{La}_2\text{Sn}_2\text{O}_7$ and Sn phases are shown in Figure S4 (Supporting Information), yielding a composition of 13% metallic Sn at 14.1 GPa. With further pressure increase, the metallic Sn content remained stable and then increased above 19.2 GPa. $\text{La}_2\text{Sn}_2\text{O}_7$ remained in a pyrochlore structure

despite small amounts of Sn loss.^[22,23] Therefore, our X-ray diffraction results reveal that a small amount of metallic tin forms by chemical decomposition at 2.0 GPa like $\text{Cd}_2\text{Nb}_2\text{O}_7$. Here, we deduce that the pressure-induced visible multinarrow PL at this pressure may be related to the lattice distortion caused by phase decomposition.

We investigated the evolution of the electronic states with structural changes using typical Nyquist plots of $\text{La}_2\text{Sn}_2\text{O}_7$ at different pressures up to 35.6 GPa, as shown in Figure 3a. Two semicircles can be seen clearly, which represent the grain and grain boundary contribution to the total resistance. We modeled the impedance spectroscopy with an equivalent circuit consisting of a resistor and constant phase element (CPE),^[24] expressed by $Z = 1/[T(j\omega)^P]$ and defined by two values T and P , where T is the capacitance component units and j and ω are the imaginary unit and frequency, respectively. We placed a CPE in parallel to the resistance to produce a Cole element. By fitting the data of the circuit parameters using ZView impedance analysis software,^[25] we obtained the grain resistance (R) values as a function of pressure in Figure 3b. Near 2.6 GPa, R obviously drops by one order of magnitude, possibly due to crystal lattice shrinkage reducing the La–O2 distance with pressure, which implies overlapping between the La t_{2g} and O2 2p orbital that broadens the conduction band (CB) and lowers the resistance.^[26] However, here, the main reason for this was due to phase decomposition-produced vacancies that allow hole conduction; the system resistance decreased at 2.6 GPa and then R increased with increasing pressure due to pressure-enhanced trigonal distortion. Consequently, this opened a full gap at the Fermi energy above 2.6 GPa. The electronic structure of $\text{La}_2\text{Sn}_2\text{O}_7$ can be explained by the electronic structure of the $\text{Sn}_2\text{O}_6^{4-}$ octahedral corner-sharing network and the conduction

band of $\text{La}_2\text{Sn}_2\text{O}_7$ is formed from the antibonding Sn 5s–O 2p caused by the distortion of the Sn–O–Sn bonds. Therefore, the reduction of the Sn–O–Sn angle from 133° to 126° below 23.7 GPa strongly affected the electrical properties of $\text{La}_2\text{Sn}_2\text{O}_7$, leading to a relatively narrow conduction band and a wide bandgap that caused R to increase by four orders of magnitude from 2.6 to 22.1 GPa, which is also associated with PL enhancement. Above this pressure, the PL quenched and was accompanied by a sudden increase in the Sn–O1–Sn angle and an almost stable R value. $\text{La}_2\text{Sn}_2\text{O}_7$ is a semiconductor at RT and it becomes an oxygen ion conductor at high temperatures with a conductivity of $1.7 \times 10^{-5} \Omega^{-1} \text{cm}^{-1}$ at 800°C .^[27] Thus, the increase of R indicated a pressure-induced semiconductor–insulator transition and this transition was associated with the novel PL.

We also used first-principles calculations to investigate the electronic structure of pyrochlore $\text{La}_2\text{Sn}_2\text{O}_7$ with pressure. At ambient pressure, the calculated bandgap of $\text{La}_2\text{Sn}_2\text{O}_7$ was 3.38 eV, which is consistent with the reported 3.3 eV in the literature.^[14] We calculated the partial density of states and the bandgap is shown in Figure S5 (Supporting Information). From this, we discovered bandgap closure followed by bandgap opening above 2 GPa, where PL appeared at the gap-reversal turning point. The pressure-induced semiconductor–insulator transition can be explained by the 1D E versus k diagram. The bottom of the $\text{La}_2\text{Sn}_2\text{O}_7$ CB was predominantly contributed by the Sn 5s orbital and the top of the valence band (VB) was dominated by the O 2p orbital. Thus, a larger bandgap originated from the distortion of the Sn–O1–Sn angle. These results are consistent with our AC impedance spectroscopy measurement.

Raman is sensitive to local symmetry distortion and can thus give some insight into novel PL with crystal symmetry.

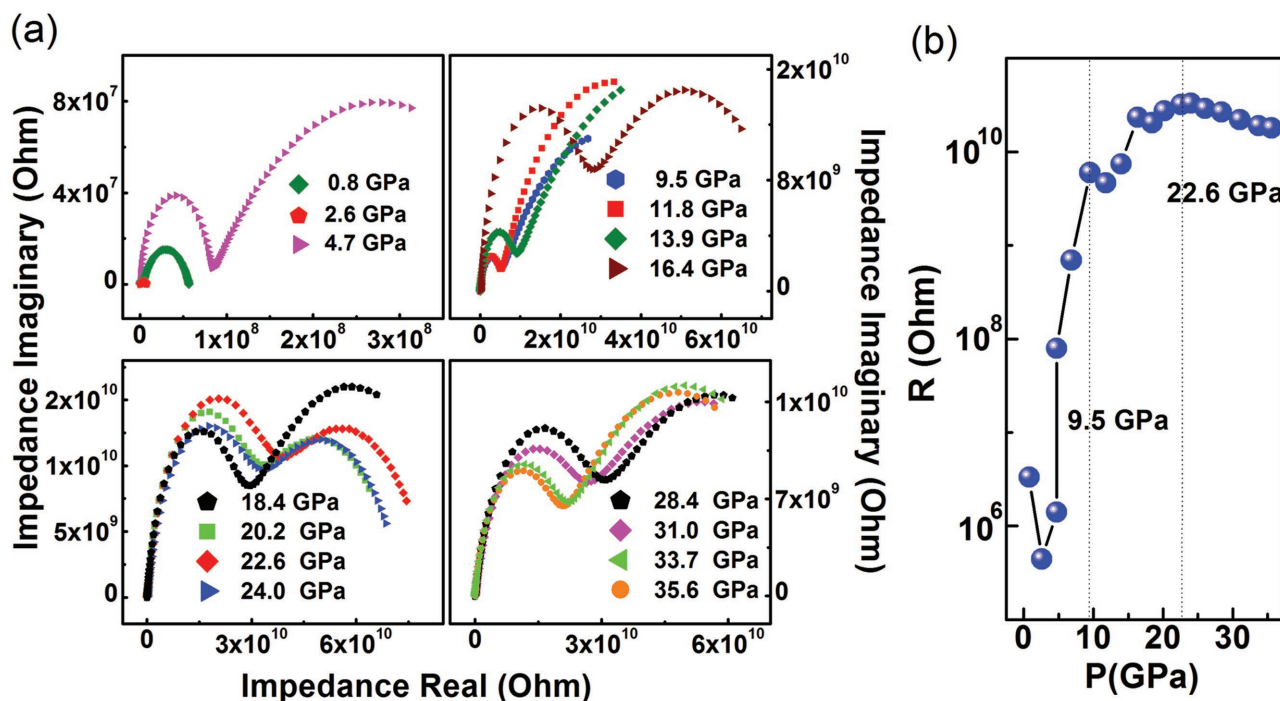


Figure 3. High-pressure AC impedance measurement of $\text{La}_2\text{Sn}_2\text{O}_7$ up to 35.6 GPa. a) The Nyquist plots of impedance spectroscopy at various pressures. b) The pressure dependence of the grain resistance R shows a four order of magnitude increase in R from 2.6 to 22.6 GPa.

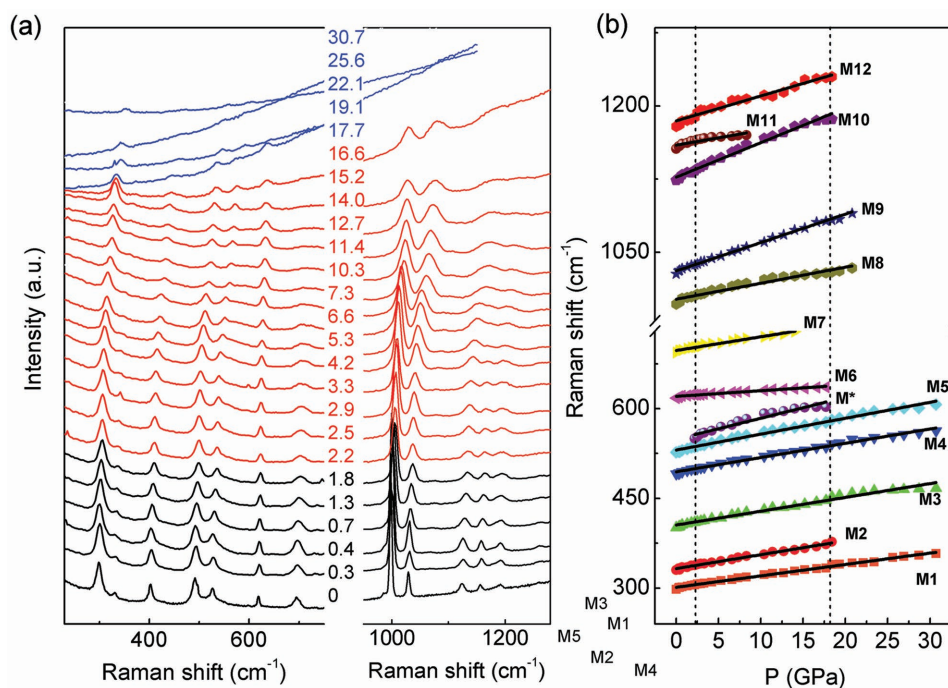


Figure 4. a) Representative Raman spectra at different pressures in $\text{La}_2\text{Sn}_2\text{O}_7$. b) Pressure dependence of Raman frequency shifts.

We conducted a systematic high-pressure Raman study between 100 and 1300 cm^{-1} at RT. Representative Raman spectra of $\text{La}_2\text{Sn}_2\text{O}_7$ at high pressure and the frequency shifts are shown in **Figure 4a,b**. Factor group analysis gave six Raman active modes $A_{1g} + E_g + 4F_{2g}$ of the pyrochlore structure. However, 12 Raman modes appeared in the Raman spectra at ambient pressure and only six of them could be assigned to the pyrochlore structure according to factor group analysis. The other Raman modes have not been observed in previous works. The assignment of these Raman modes in $\text{La}_2\text{Sn}_2\text{O}_7$ is listed in Table S1 (Supporting Information),^[16] along with a summary of the frequencies ω_0 , pressure coefficient A , and Grüneisen parameter γ of the different modes. Here, the origin of these other unidentified Raman modes may be related to phonon–phonon anharmonic interactions in the SnO_6 octahedra through the Sn–O–Sn exchange effect.^[21] The ambient-pressure frequencies are denoted as follows: M1(298 cm^{-1}), M2(330 cm^{-1}), M3(401 cm^{-1}), M4(491 cm^{-1}), M5(527 cm^{-1}), M6(618 cm^{-1}), M7(695 cm^{-1}), M8(999 cm^{-1}), M9(1031 cm^{-1}), M10(1125 cm^{-1}), M11(1157 cm^{-1}), and M12(1179 cm^{-1}). The Raman peaks M2, M3, and M5 are F_{2g} modes representing La–O bond stretching and Sn–O bond stretching. The M7 mode can be assigned to a distortion of the SnO_6 octahedron.^[28] Here, we assigned the peak at 299 cm^{-1} to an E_g mode and the peak at 493 cm^{-1} corresponded to an A_{1g} mode. E_g symmetry was related to Sn_4O tetragonal lattice distortion and A_{1g} originated from the bending vibrations of the SnO_6 octahedron.^[19] Under high pressure, one new peak appeared near 550 cm^{-1} named M^* at 2.2 GPa and then completely disappeared at 16.6 GPa (Figure S6, Supporting Information). Between 2.2 and 23.7 GPa, the Raman M10 and M11 modes combined into one peak at 7.3 GPa and all the Raman peaks above 999 cm^{-1} disappeared one by one, which is

consistent with the pressure regions of the PL emergence and disappearance. Above 23.7 GPa, only four of the pyrochlore Raman peaks existed where we observed SnO_6 octahedral rearrangement. Therefore, we believe that Raman modes M6 and M8–M12 are related to the vibration of the SnO_6 octahedra and depended on the changes of the Sn–O–Sn bond angle. All the Raman modes shifted to higher frequencies linearly upon further compression. Upon decompression, the spectroscopic changes were partially reversible immediately and the high-pressure mixed phase fully reverted to the original structure. Therefore, a structural transition can occur by pressure and lattice distortion, resulting in a change of the point group symmetry that leaves the cubic lattice unchanged.

Three kinds of PL were distinct in different pressure gradients (**Figure 5**). Our high-pressure visible narrow-band PL results demonstrate a well-defined pressure window (6.6–16.6 GPa) that yielded flat maximum PL and sharp edges at both ends, which may provide a great calibration tool for pressure sensors at extreme conditions. This unexpected appearance of visible PL in $\text{La}_2\text{Sn}_2\text{O}_7$ was attributed to lattice distortion induced by phase decomposition above 2 GPa, where we observed a new Raman peak M^* . These unusual behaviors imply a large overlap between the Sn $5s^2$ ground state and the $5s5p$ excited state, originating from the decreasing Sn–O–Sn exchanging angle θ upon passing from 133° to 126° and thus enhancing the Sn $5s5p$ to $5s^2$ transfer rate at high pressure. Therefore, pressure-induced visible PL in $\text{La}_2\text{Sn}_2\text{O}_7$ mainly originates from a reduction of the Sn–O–Sn exchange interaction that enhances the 3P_1 , 3P_2 , $^1P_1 \rightarrow ^1S_0$ photon transitions at high pressure, where 1S_0 is expressed as the Sn $5s^2$ ground state and 3P_1 , 3P_2 , and 1P_1 are the $5s5p$ first excited states.^[29] Here, we give the energy level scheme for the s^2 ions from the ligand field model in $\text{La}_2\text{Sn}_2\text{O}_7$, as shown in the Figure 5 inset.

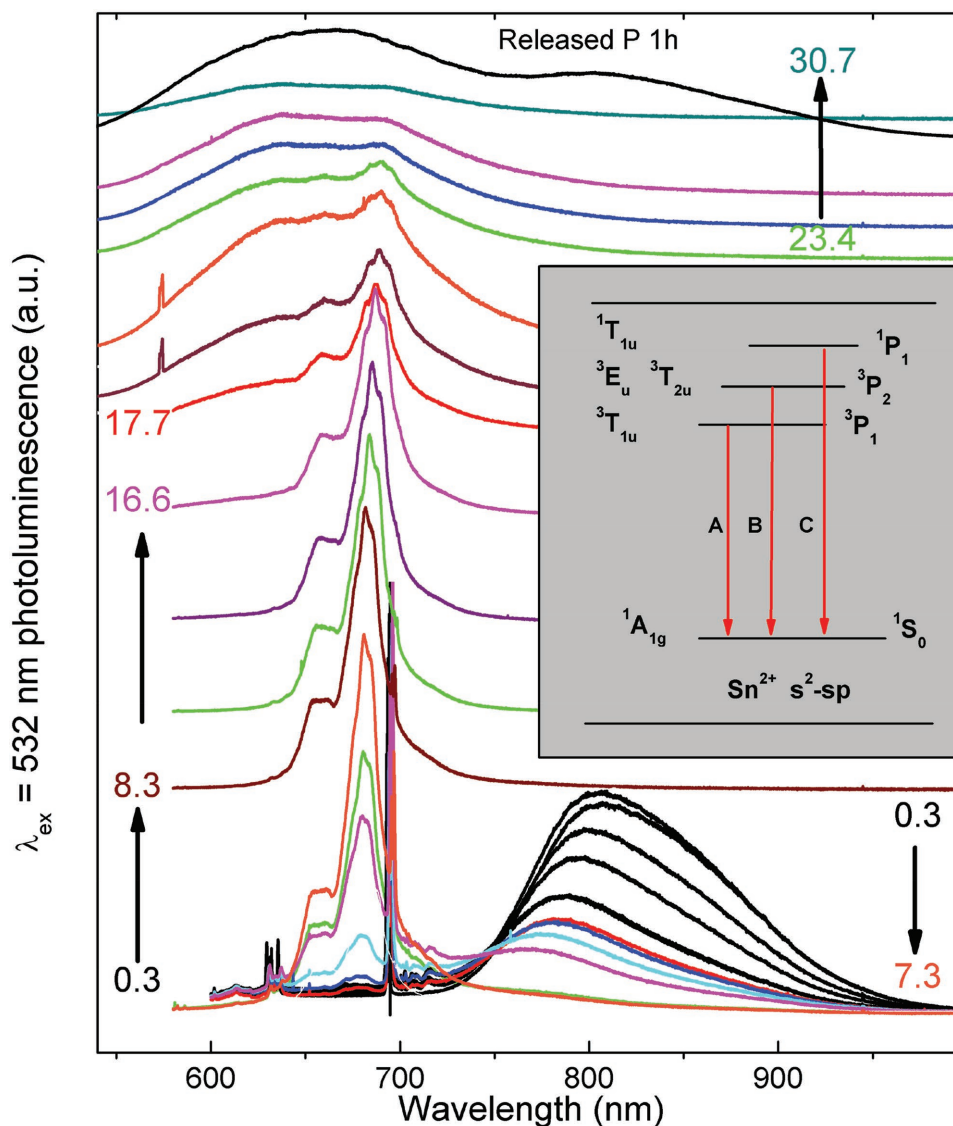


Figure 5. Emission spectra of $\text{La}_2\text{Sn}_2\text{O}_7$ under high pressure. The inset is the energy level scheme for the Sn^{2+} ions with the s^2 ground-state configuration in $\text{La}_2\text{Sn}_2\text{O}_7$, which is classified as an s^2 -sp transition.

The Sn s^2 ground-state configuration is $^1A_{1g}$, while the first excited configuration is t_{1u} , which leads to the states $^3A_{1u}$, $^3T_{1u}$, 3E_u , $^3T_{2u}$, and $^1T_{1u}$. The transition of $A_{1g} \rightarrow ^3A_{1u}$ is forbidden. The next four energy levels corresponding to $A_{1g} \rightarrow ^3T_{1u}$, $A_{1g} \rightarrow ^3E_u + ^3T_{2u}$, $A_{1g} \rightarrow ^1T_{1u}$ are the A band ($^1S_0 \rightarrow ^3P_1$) at 681 nm (1.82 eV), B band ($^1S_0 \rightarrow ^3P_2$) at 659 nm (1.88 eV), and C band ($^1S_0 \rightarrow ^1P_1$) at 635 nm (1.95 eV), respectively.^[30,31] The multiband PL peaks in $\text{La}_2\text{Sn}_2\text{O}_7$ were classified as an s^2 -sp transition, while the energy levels of the valence s and p orbitals were sensitive to ligand field effects. Above 16.6 GPa, another broad PL emerged near 661 nm (1.87 eV) and existed to the highest pressure of 30.7 GPa. This PL originates from the oxygen vacancies and the O-related defects.^[32] Upon decompression and relaxation at ambient pressure for 1 h, this peak remained, but the NIR PL recovered.

Our main conclusions of the present work are as follows: first, an unusual near-infrared PL was observed in $\text{La}_2\text{Sn}_2\text{O}_7$

at ambient pressure that was associated with the defect level of Sn^{2+} ions. Second, pressure-induced visible narrow-band PL was found in $\text{La}_2\text{Sn}_2\text{O}_7$ at RT and 2 GPa. The emergence of this anomalous PL behavior was associated with lattice symmetry distortion by phase decomposition, where a decrease of the Sn–O1–Sn exchanging angle θ below 130° enhanced the PL quantum yield leading to the Sn $^3P_1 \rightarrow ^1S_0$, $^3P_2 \rightarrow ^1S_0$, $^1P_1 \rightarrow ^1S_0$ photon transitions and strengthening below 23.7 GPa. However, the sudden increase of the Sn–O1–Sn angle beyond 130° at 25 GPa by the rearrangement of the SnO_6 octahedron caused a reduction of the PL quantum yield and quenched PL. Therefore, the Sn–O1–Sn bond angle was severely bent between 2 and 23.7 GPa, which is crucial for pressure-induced PL. Third, a pressure-induced semiconductor–insulator transition occurred above 2 GPa and this transition was associated with the novel visible PL. We discovered bandgap closure followed by bandgap opening, while at the turning point of the gap reversal, novel

visible PL appeared. Our findings highlight the role of pressure in obtaining PL in concentrated materials at room temperature and provide new insight into improving photoluminescent materials.

Experimental Section

Samples of $\text{La}_2\text{Sn}_2\text{O}_7$ were synthesized with a solid-state reaction (SSR). The SnO_2 (99.9% in purity) and La_2O_3 (99.9%) powders were weighed according to the stoichiometric ratio. The in situ high-pressure X-ray diffraction ($\lambda = 0.3100 \text{ \AA}$) measurement was performed with an ADXRD mode at beamline 16BM-D of the Advanced Photon Source, Argonne National Laboratory. The as-prepared samples were loaded into a gasketed diamond anvil cell (DAC) with a 16:3:1 methanol/ethanol/water mixture as a pressure-transmitting medium. The high-pressure Raman spectroscopy was measured with a 532 nm laser at the Center for High Pressure Science and Technology Advanced Research (HPSTAR). The PL spectral measurement of $\text{La}_2\text{Sn}_2\text{O}_7$ used an Nd-YAG 532 nm laser and an optical grating of 1200 g mm^{-1} . In all high-pressure experiments, pressure was calibrated by the ruby luminescence method.^[33] Van der Pauw electrodes were integrated on one facet of the DAC for the electrical property measurement under high pressure. The fabrication process of the detecting microcircuit was described in previous publications.^[34] The AC impedance spectroscopy measurements in the frequency range of 1 Hz to 10 MHz at pressures up to 35.6 GPa were carried out using a Solartron 1260 impedance analyzer equipped with a Solartron 1296 dielectric interface. The applied AC voltage was 0.1 V.

The first-principles calculations under high pressure were based on the spin-polarized DFT implemented in the CASTEP code.^[35] The exchange-correlation potentials were treated with the local density approximation (LDA) parameterized by the Ceperley–Alder–Perdew–Zunger (CAPZ) function.^[36,37] The plane-wave kinetic energy cutoff used was 1000 eV. The electronic interactions were described using ultrasoft pseudopotentials.^[38] The neighboring planes were separated by at least 15 Å in the hexagonal supercells. The XPS spectra were recorded on powders with Axis Ultra DLD spectrometer using an Al K_{α} monochromatized source.

Supporting Information

Supporting Information is available from the Wiley Online Library or from the author.

Acknowledgements

This work was financially supported by the National Nature Science Foundation of China (Grant Nos. 11534003 and 51527801), NSAF (Grant No. U1530402), and open project of State Key Laboratory of Superhard Materials (Jilin University). HPCAT operations were supported by DOE-NNSA under Award No. DE-NA0001974 and DOE-BES under Award No. DE-FG02-99ER45775 with partial instrumentation funding by NSF. APS was supported by DOE-BES under Contract No. DE-AC02-06CH11357. W.Y. acknowledges financial support from the DOE Basic Energy Sciences (BES) X-ray Scattering Core Program (DE-FG02-99ER45775).

Conflict of Interest

The authors declare no conflict of interest.

Keywords

high pressure, insulating state, lattice distortion, phase decomposition, photoluminescence

Received: March 17, 2017

Revised: May 13, 2017

Published online:

- [1] M. Ramuz, B. C. K. Tee, J. B. H. Tok, Z. Bao, *Adv. Mater.* **2012**, *24*, 3223.
- [2] W. Q. Shi, L. Y. Yuan, C. Z. Wang, L. Wang, L. Mei, C. L. Xiao, L. Zhang, Z. J. Li, Y. L. Zhao, Z. F. Chai, *Adv. Mater.* **2014**, *26*, 7807.
- [3] K. Sickafus, L. Minervini, R. Grimes, J. Valdez, M. Ishimaru, F. Li, K. McClellan, T. Hartmann, *Science* **2000**, *289*, 748.
- [4] J. S. Gardner, M. J. Gingras, J. E. Greedan, *Rev. Mod. Phys.* **2010**, *82*, 53.
- [5] I. Mirebeau, I. Goncharenko, P. Cadavez-Peres, S. Bramwell, M. Gingras, J. Gardner, *Nature* **2002**, *420*, 54.
- [6] F. F. Tafti, J. J. Ishikawa, A. McCollam, S. Nakatsuji, S. R. Julian, *Phys. Rev. B* **2012**, *85*, 205104.
- [7] I. Loa, P. Adler, A. Grzechnik, K. Syassen, U. Schwarz, M. Hanfland, G. K. Rozenberg, P. Gorodetsky, M. P. Pasternak, *Phys. Rev. Lett.* **2001**, *87*, 125501.
- [8] Y. Zhao, W. Yang, N. Li, Y. Li, R. Tang, H. Li, H. Zhu, P. Zhu, X. Wang, *J. Phys. Chem. C* **2016**, *120*, 9436.
- [9] H. Mizoguchi, P. M. Woodward, C.-H. Park, D. A. Keszler, *J. Am. Chem. Soc.* **2004**, *126*, 9796.
- [10] P. Ranby, D. Mash, S. Henderson, *Br. J. Appl. Phys.* **1955**, *6*, S18.
- [11] I. Hernández, F. Rodríguez, H. D. Hochheimer, *Phys. Rev. Lett.* **2007**, *99*, 027403.
- [12] S. L. Ko, S. Park, C.-W. Kim, D. Lee, M.-S. Choi, C. Lee, C. Jin, *Appl. Phys. A* **2015**, *121*, 715.
- [13] W. Williamson III, S. Lee, *Phys. Rev. B* **1991**, *44*, 9853.
- [14] H. Mizoguchi, H. W. Eng, P. M. Woodward, *Inorg. Chem.* **2004**, *43*, 1667.
- [15] W. M. Yen, H. Yamamoto, *Phosphor Handbook*, CRC Press, Boca Raton, FL, USA **2006**.
- [16] L. Kong, I. Karatchevtseva, M. G. Blackford, N. Scales, G. Triani, E. Vance, *J. Am. Ceram. Soc.* **2013**, *96*, 2994.
- [17] A. C. Larson, R. B. Von Dreele, *General Structure Analysis System*, LANSCE, MS-H805, Los Alamos, NM, USA **1994**.
- [18] A. Salamat, R. Briggs, P. Bouvier, S. Petitgirard, A. Dewaele, M. E. Cutler, F. Corà, D. Daisenberger, G. Garbarino, P. F. McMillan, *Phys. Rev. B* **2013**, *88*, 104104.
- [19] B.-J. Yang, Y. B. Kim, *Phys. Rev. B* **2010**, *82*, 085111.
- [20] S. Saha, D. Muthu, C. Pascanut, N. Dragoe, R. Suryanarayanan, G. Dhalenne, A. Revcolevschi, S. Karmakar, S. Sharma, A. Sood, *Phys. Rev. B* **2006**, *74*, 064109.
- [21] S. Saha, D. S. Muthu, S. Singh, B. Dkhil, R. Suryanarayanan, G. Dhalenne, H. Poswal, S. Karmakar, S. M. Sharma, A. Revcolevschi, *Phys. Rev. B* **2009**, *79*, 134112.
- [22] F. Zhang, J. Lian, U. Becker, R. C. Ewing, L. Wang, L. A. Boatner, J. Hu, S. Saxena, *Phys. Rev. B* **2006**, *74*, 174116.
- [23] C. R. Stanek, L. Minervini, R. W. Grimes, *J. Am. Ceram. Soc.* **2002**, *85*, 2792.
- [24] F. B. Growcock, R. J. Jasinski, in *Oil-Field Chemistry: Enhanced Recovery and Production Stimulation*, Vol. 396, (Ed. J. K. Borchardt, T. F. Yen), American Chemical Society, Washington DC, USA **1989**, pp. 636–650.
- [25] D. Johnson, *ZView: a Software Program for IES Analysis, Version 2.8*, Scribner Associates, Inc., Southern Pines, NC, USA **2002**, p. 200.
- [26] P. Velasco, J. Alonso, V. Tissen, W. Marshall, M. Casais, M. Martinez-Lope, A. de Andrés, C. Prieto, J. Martinez, *Phys. Rev. B* **2003**, *67*, 104403.

- [27] Y. Mao, G. Li, W. Xu, S. Feng, *J. Mater. Chem.* **2000**, *10*, 479.
- [28] M. Vandenborre, E. Husson, J. Chatry, D. Michel, *J. Raman Spectrosc.* **1983**, *14*, 63.
- [29] R. Ropp, R. Mooney, *J. Electrochem. Soc.* **1960**, *107*, 15.
- [30] M. Fang, X. Tan, B. Cheng, L. Zhang, *J. Mater. Chem.* **2009**, *19*, 1320.
- [31] T. Tsuboi, M. J. Stillman, P. W. M. Jacobs, *Chem. Phys. Lett.* **1980**, *74*, 135.
- [32] S. Luo, P. K. Chu, W. Liu, M. Zhang, C. Lin, *Appl. Phys. Lett.* **2006**, *88*, 183112.
- [33] H. Mao, J.-A. Xu, P. Bell, *J. Geophys. Res.: Solid Earth* **1986**, *91*, 4673.
- [34] Y. Han, C. Gao, Y. Ma, H. Liu, Y. Pan, J. Luo, M. Li, C. He, X. Huang, G. Zou, *Appl. Phys. Lett.* **2005**, *86*, 064104.
- [35] M. Segall, P. J. Lindan, M. a. Probert, C. Pickard, P. Hasnip, S. Clark, M. Payne, *J. Phys.: Condens. Matter* **2002**, *14*, 2717.
- [36] D. M. Ceperley, B. Alder, *Phys. Rev. Lett.* **1980**, *45*, 566.
- [37] J. P. Perdew, A. Zunger, *Phys. Rev. B* **1981**, *23*, 5048.
- [38] D. Vanderbilt, *Phys. Rev. B* **1990**, *41*, 7892.